The Evolution of MXenes Conductivity and Optical Properties Upon Heating in Air

Ahmad A. Shamsabadi[1, #], Hui Fang[1, #], Danzhen Zhang[2], Anupma Thakur[3], Cindy Y. Chen[1], Aixi Zhang[1], Haonan Wang[1], Babak Anasori[3,4], Masoud Soroush[5], Yury Gogotsi[2], and Zahra Fakhraai[1, *]

[1]Department of Chemistry, University of Pennsylvania, Philadelphia, Pennsylvania 19104, United States

[2]A.J. Drexel Nanomaterials Institute and Department of Material Science and Engineering, Drexel University, Philadelphia, Pennsylvania 19104, United States

[3]Department of Mechanical and Energy Engineering and Integrated Nanosystems Development Institute, Purdue School of Engineering and Technology, Indiana University–Purdue University Indianapolis, Indiana 46202, United States

[4]School of Materials Engineering, Purdue University, West Lafayette, IN 47907, United States

[5]Department of Chemical and Biological Engineering, Drexel University, Philadelphia, Pennsylvania 19104, United States

REVISED VERSION

October 2, 2023

Submitted for Publication in *Small Methods*

[#]These authors contributed equally to this work.

*Corresponding author: fakhraai@sas.upenn.edu

Abstract

MXenes, a family of two-dimensional (2D) transition metal carbides and nitrides, have excellent electrical conductivity and unique optical properties. However, MXene 2D flakes can be oxidized in air at ambient temperature, and the oxidation is accelerated upon heating. Intercalation of water may cause hydrolysis, accelerating the oxidation. The oxidation affects many properties of MXenes. Developing new tools to readily characterize MXenes' thermal stability can enable deeper insights into their structure-property relationships. Here, we employ in-situ spectroscopic ellipsometry (SE) to characterize the optical properties of three types of MXenes ($Ti_3C_2T_x$, $Mo_2TiC_2T_x$, and Ti_2CT_x) with varied composition and atomistic structures and at different temperatures, and investigate the MXenes' thermal degradation under ambient environment. We demonstrate that changes in MXene extinction and conductivity in the visible and near-IR regions correlate well with the amount of intercalated water and hydroxyl termination groups and the level of MXene oxidation, measured using thermogravimetric (TGA) analysis. As such, MXene degradation can be monitored through measuring optical conductivity. It is found that among the three MXenes, $Ti_3C_2T_x$ and Ti_2CT_x, respectively, have the highest and lowest thermal stability, indicating the role of transition metal type, MXene synthesis route, and the number of atomic layers in 2D flakes. Our findings demonstrate the utility of SE as a powerful in-situ technique for rapid structure-property relationship studies and pave the way for the further design, fabrication, and property optimization of novel MXene materials.

KEYWORDS: MXenes, optical properties, optical conductivity, thermal stability, spectroscopic ellipsometry.

Introduction

MXenes are two-dimensional (2D) materials with a unique combination of conductivity and interactions with electromagnetic waves, including visible light, arising from the free electrons of their metal-carbide/nitride backbone. Due to these properties, MXenes and MXene-based composites have appealing electrical and optical properties[1-4] and have been successfully used for the assembly of functional devices for electronic and photonic applications, such as energy storage,[5-8] optoelectronics,[9-11] chemical sensing,[12-14] wireless communications,[15] catalysis,[16] and wearable electronics.[17] MXenes have the general formula of $M_{n+1}X_nT_x$, where M signifies an early transition metal, X is carbon and/or nitrogen, n =1–4, and T denotes surface functional groups (–OH, =O, –Cl, –F, etc.).[2, 18] Since the first discovery of $Ti_3C_2T_x$,[19] the prototypical MXene, around 50 different MXenes have been synthesized from a variety of precursors and etchants following various synthesis pathways.[20-27] Diverse optical properties can be obtained from MXenes with varied structures and compositions, and prepared using different synthesis and etching pathways.

MXenes have high free electron density (*e.g.*, 2 x 10^{21} cm^{-3} for $Ti_3C_2T_x$),[28] making them excellent candidates for nanoelectronics devices,[29] and affording them diverse and tunable optical properties. For example, MXenes have been shown to support surface plasmon (SPR) resonances,[30] and localized surface plasmon resonances (LSPR) in small-size,[31] and $Ti_3C_2T_x$ shows a strong and tunable absorption band in the near IR region of the spectrum.[32] Density functional theory (DFT) calculations suggest that this peak can be due to an optically active inter-band transition in $Ti_3C_2T_x$, due to the excellent light confinement at flake surfaces,[33, 34] which can vary with surface terminations. These calculations predict that the intrinsic plasmon resonance of $Ti_3C_2T_x$ MXenes are located at higher energy, around ~10 eV.[33, 34] On the other hand, ultrafast transmittance and reflectance studies in $Ti_3C_2T_x$ favor a plasmon resonance assignment for this peak, as the observed transient signal in the corresponding spectral region (800 nm for $Ti_3C_2T_x$) is consistent with a plasmonic behavior and can be distinct from the kinetics observed in the high energy inter-band peaks.[35]

Nevertheless, the strong near-IR absorption peak is continuously tunable upon applied voltage and blueshifts under reduction conditions by ~100 nm in $Ti_3C_2T_x$ films, when used as cathodes in electrochromic devices.[36, 37] Theoretical calculations have further demonstrated that besides structure, transition-metal and X atom (carbon, nitrogen, or oxygen substitution) compositions, functional groups on MXene surfaces (T_x surface terminations) can also play an important role in tuning their electronic and optical properties,[38] which is also supported by a few experimental studies.[39-41] However, using surface terminations to control optical properties can

be challenging, as approaches such as controlling surface chemistry through annealing under low-pressure O_2, vacuum, inert gases such as Ar, and oxygen plasma treatment, to modify the ratio of oxygen and hydroxyl terminations, can also lead to the formation of transition metal oxides and thus degradation of MXene, especially at high temperatures.[39, 41, 42]

The oxidative degradation of MXenes during storage and device fabrication results in unfavorable changes in their electrical conductivity, optical properties, and, thus, performance in many applications. Numerous studies have demonstrated that MXene colloidal solutions have poor chemical stability due to the structural transformation caused by oxygen and water molecules, resulting in undesired hydrolysis, oxidation, and degradation.[43-47] Studies of the oxidation of MXene films under different atmospheric environments,[48, 49] have shown that increasing temperature can accelerate the rate of the oxidation reaction.[39, 45] When MXene films are annealed in air, two distinct changes can be observed in their properties. At low temperatures (up to 300 ºC), the intercalated H_2O and other physically adsorbed molecules are removed while the MXene structure is maintained.[39, 50 ,51] At higher temperatures, surface de-functionalization and oxidation can occur simultaneously, forming transition metal oxide, CO_2, and water.[52] In $Ti_3C_2T_x$ MXene, anatase TiO_2 nanocrystals supported on amorphous carbon sheets were formed upon thermal degradation, which transformed into rutile TiO_2 nanocrystals as the oxidation temperature was further increased.[53, 54]

As electro-optical properties of MXenes vary with the changes in their free electron density, MXenes' optical information can be used as a tool to monitor their oxidation, as well as other processes that can affect their surface termination and oxidation state of the transition metal. Spectroscopic ellipsometry (SE) is a robust non-destructive technique that can be used to measure the optical properties, dielectric constant, film thickness, and conductivity of MXenes[10, 55] and other 2D materials[56, 57], as well as organic-inorganic hybrid composites[58, 59] in the visible and near-IR spectral range. SE has been previously used to characterize MXene properties such as film thickness, surface coverage or uniformity[60], optical properties[10, 32, 61], and conductivity[35, 55]. The onset of free carrier oscillations and conductivity of ultra-thin $Ti_3C_2T_x$ films were also determined using this technique.[10, 61] While the refractive index (n), extinction coefficient (k), electrical conductivity, and the associated scattering of $Ti_3C_2T_x$ thin films can be measured using SE, there are some uncertainties in the choice of parameters used for modeling these data. For example, both Harmonic[10] and Lorentz-type[35, 61] oscillators have been used to fit the two extinction energy peaks in the UV to the visible spectral region for $Ti_3C_2T_x$ films, which can result in slight variations in the predicted absorption spectra. Nevertheless, the optical conductivity (or resistivity)

of MXenes can be obtained from SE data in the near-IR region, typically fitted using Drude oscillator. Given that $Ti_3C_2T_x$ MXene resistivity is increased upon oxidation[62, 63], and in-situ SE can readily measure optical resistivity [59, 64], for the first time, we proposed using in-situ SE to monitor MXenes oxidation.

In this study, we employ in-situ SE measurements to study the evolution of the optical properties of three types MXenes, $Ti_3C_2T_x$, $Mo_2TiC_2T_x$, and Ti_2CT_x, with varied composition and atomistic structure, upon annealing to 600 °C under ambient conditions. We demonstrate that changes in the extinction coefficient and optical resistivity of these MXenes can be correlated with the desorption of water and loss of hydroxyl groups at temperatures below 200 °C as well as their oxidative degradation at higher temperatures, as measured through thermogravimetric (TGA) analysis. In-situ SE experiments provide a non-contact method to measure MXene conductivity, oxidation state, and durability, which can also be applied in thin-film conditions, on small amounts of materials, and inside multi-layer geometries, providing a rapid method for quality control and process optimization in applications where oxidation stability is critical.

Results and Discussions

Optical properties of MXenes at room temperature. Three types of MXenes, with different compositions and number of atomic layers (n = 1 and 2) were chosen in this study, $Ti_3C_2T_x$, $Mo_2TiC_2T_x$, and Ti_2CT_x (structures shown in **Figure 1a**), with strong differences in their thermal stability and optical properties in the visible to near-infrared (NIR) spectral regions.[32] Selection of these MXenes allowed us to explore the effect of the surface transition metal (Ti vs Mo) and the number of atomic layers ($M_3C_2T_x$ vs M_2CT_x) in the MXene structure. $Ti_3C_2T_x$ and Ti_2CT_x were synthesized by selective removal of aluminum from their corresponding MAX phases (**Figures S1&S2**), resulting in –OH, –F, and =O surface terminations and H_2O and Li^+ intercalation.[7, 24] $Mo_2TiC_2T_x$ was prepared using HF and tetramethylammonium hydroxide (TMAOH) solutions as the etchant and intercalant, respectively.[65] This method reduces the concentration of the –F termination and results in the intercalation of tetramethylammonium (TMA^+) and H_2O. TMA^+ is a large organic ion that can significantly increase inter-flake spacing and electrical resistance.[66] More details of synthesis and purification can be found in the Materials and Methods section. Full etching of the aluminum element of all three MXenes was corroborated in X-ray diffraction (XRD) analysis, by the position of the (002) peak and the absence of residual peaks of the MAX phases in the diffraction patterns (**Figure S3** in SI). These XRD patterns and

SEM image (**Figure S4**) were similar to previous studies, indicating the complete exfoliation of MXene flakes.[65]

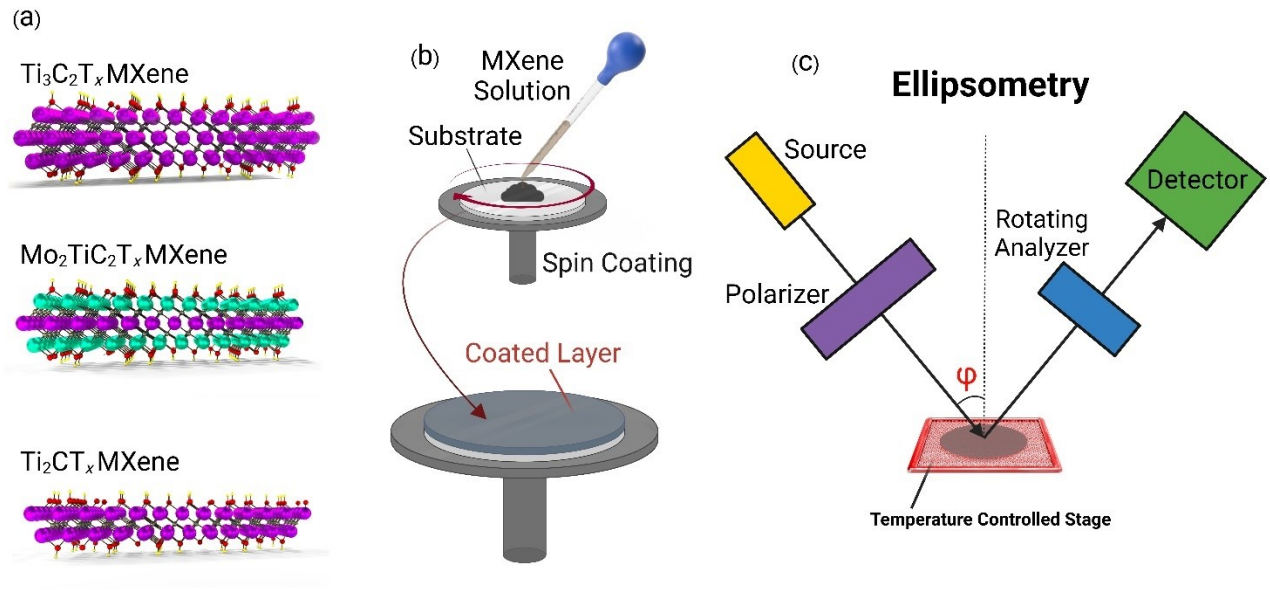

Figure 1. (a) Crystal structures of MXenes used in this study, (Ti: pink. Mo: green, and C: black), **(b)** Schematic of preparation of MXene films via spin coating, and **(c)** Schematic geometry of in-situ variable-angle spectroscopic ellipsometry measurements. φ indicates the angle of incidence of the ellipsometer beam, which was held at 70° for in-situ experiments.

To determine the optical properties of the synthesized MXenes, ultrathin MXene films were fabricated on frosted glass substrates via spin-casting from aqueous suspensions (**Figure 1b**). Variable-angle spectroscopic ellipsometry (SE) measurements were performed on these samples at room temperature. For in-situ experiments, the angle of incidence was held at 70° (**Figure 1c**, more details in Materials and Methods as well as SI). Spectroscopic ellipsometry angles $\Psi(\lambda)$ and $\Delta(\lambda)$ were collected over a spectral range of 370 nm < λ < 1600 nm. An example of the measured $\Psi(\lambda)$ and $\Delta(\lambda)$ at various angles of incidence for $Ti_3C_2T_x$ film is shown in **Figures 2a, b**, where the sample was synthesized based on our new optimized synthesis procedures.[67] The results for regular synthesized $Ti_3C_2T_x$ (described in experimental section) and the other two MXenes, which was used for the following in-situ ellipsometry, measured at 70° incidence angle are shown in

Figures S9-S11 of SI. The measured SE spectra were fitted to multi-layer optical models, where the MXene layer's optical properties were reconstructed using a combination of up to two Harmonic oscillators (to quantify extinction), a Drude oscillator (to quantify resistivity), and when necessary constant values at the far UV (E_∞) and far infrared (IR pole) to adjust for extinction beyond the window of measurements (more details in SI and **Tables S2** and **S3**). An alternative fitting was also explored for $Mo_2TiC_2T_x$, as detailed in SI and **Figure S11**, to explore whether a low bandgap semiconductor better describes its optical properties.[68] The resulting best-fit that globally fits all values for $\Psi(\lambda)$ and $\Delta(\lambda)$ at all angles are shown by the solid lines in **Figures 2a, b** for $Ti_3C_2T_x$, which fit the experimental data well over the entire spectral range and agrees well with the results from previous studies.[10] The predicted optical properties based on these fits, comprising the real (n) and the imaginary (k) components of the index of refraction are shown in **Figure 2c**, and the calculated real and imaginary components of the dielectric constant ($\varepsilon_1, \varepsilon_2$) are shown in **Figure 2d**.

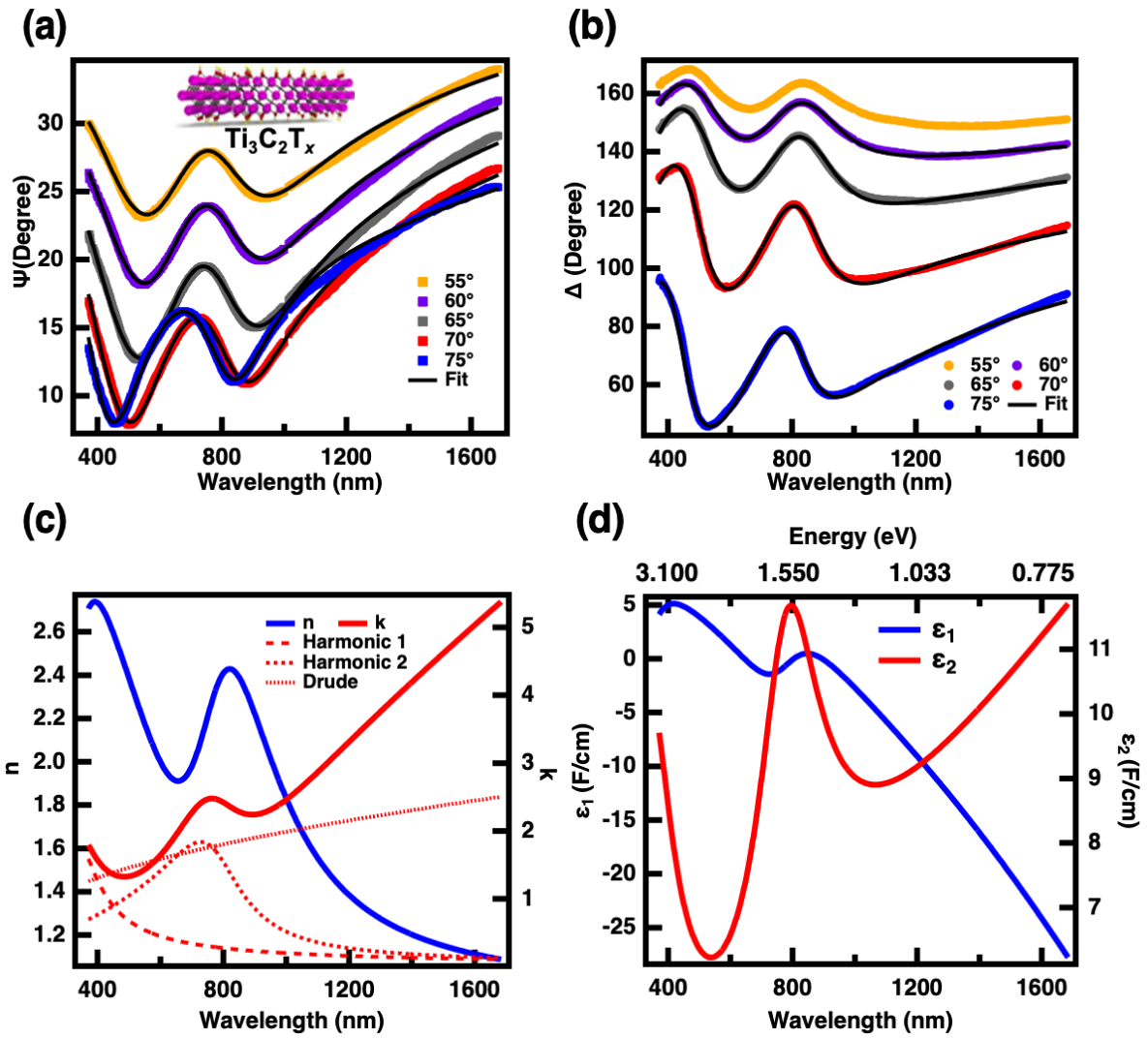

Figure 2. (a, b) Measured (squares, spheres) spectroscopic angles Ψ (squares) and Δ (spheres) along with the global best-fit (solid black lines) as a function of wavelength at various angles of incidence, 55° (orange), 60° (purple), 65° (gray), 70° (cyan), and 75° (blue), performed on an optimized $Ti_3C_2T_x$ thin film with a thickness of 14 nm. **(c)** The real (n, blue line, left axis) and imaginary (k, red solid line, right axis) components of the index of refraction, calculated based on the global fit to the SE data in **a** and **b**. The red dashed and dotted lines represent the contributing components of the three oscillators used to construct k. **(d)** Real (ε_1, blue line, left axis) and imaginary (ε_2, red line, right axis) of the dielectric constant as a function of wavelength for $Ti_3C_2T_x$ film calculated based on the data. The corresponding frequency values in eV units are shown above the graph.

As seen in **Figure 2c**, in $Ti_3C_2T_x$, the imaginary part of the index of refraction, k, which is proportional to the extinction coefficient (see more details in SI) consists of two distinct extinction peaks in the UV and visible regions of the spectrum (fitted to harmonic oscillators). It also shows

an increasing trend in extinction with increasing wavelength (fitted with a Drude oscillator) indicating DC conductivity. The harmonic 1 oscillator centered at ~3.7 eV (335 nm, **Table S2**) has been attributed to MXene inter-band transitions[33], and is also observed in the other two MXenes (4.9 eV for Ti_2CT_x and 2.6 eV for $Mo_2TiC_2T_x$ as shown in **Table S3**). In $Ti_3C_2T_x$ and Ti_2CT_x, another extinction is observed in the visible-near IR region of the spectrum (harmonic 2, ~1.6 eV, 790 nm for $Ti_3C_2T_x$ and 2.3 eV, 540 nm for Ti_2CT_x as shown in **Tables S2** and **S3).** This strong extinction has been attributed to two possible origins: inter-band transitions between closely spaced bands for surface Ti atoms or a localized surface plasmon resonance.[32] Density functional theory (DFT) calculations of both Ti_2CT_x and $Ti_3C_2T_x$ MXenes suggest that the low-energy extinction can be attributed to closely spaced inter-band transitions of the surface atoms, which can vary with surface terminations, while the intrinsic plasmon resonance of these MXenes were predicted to be at higher energy, around ~10 eV.[33, 34] Conversely, scanning transmission electron microscopy (STEM)-electron energy loss spectroscopy (EELS) measurements performed on $Ti_3C_2T_x$ flakes found that the reflection peak at ~730 nm, assigned as a transverse surface plasmon resonance (SPR), is independent of the flake size and can be shifted to higher energies in proportion to the enhanced carrier concentrations,[31] and MXene compositions.[32] This is the generally accepted assignment in the current literature. We note that, an out-of-plane localized plasmon resonance (LSPR) is expected to produce optical anisotropy in SE measurements, with a larger value out-of-plane extinction coefficient.[58] However, our variable-angle SE data shown in **Figure 2** does not fit an anisotropic optical model and is thus not consistent with an out-of-plane plasmon resonance. In contrast, an in-plane plasmon resonance (SPR or LSPR) is expected to produce a larger in-plane extinction coefficient, which was also not observed. An in-plane LSPR is also expected to strongly depend on the lateral flake size, which was not observed here or in previous studies.[31] However, given the large heterogeneity of flake sizes in this study, we are not able to independently confirm whether the location of the harmonic 2 oscillator is size-dependent, which would be required to distinguish between in-plane SPR and LSPRs. The data shown in **Figure 2c** is ensemble-averaged data on a heterogeneously sized sample, explaining the broad nature of this peak. Future experiments using multi-angle SE experiments on thicker films, with larger optical density and on size-controlled samples can help better determine the nature of this extinction, which is beyond the scope of this study.

As seen in **Figure 2d**, the real part of dielectric constant (ε_1) decreases strongly with wavelength and becomes negative around ~620 nm (energy below ~1.5 eV), indicating the onset of the free carrier oscillations. This behavior can be accurately modeled by a Drude oscillator, with an optical resistivity (conductivity) value of 0.0010 ± 0.0001 Ohm·cm (978 ± 10 S/cm) for the

14-nm-thick $Ti_3C_2T_x$ MXene film. The resistivity values of the Ti_2CT_x film (3 nm thick) and the $Mo_2TiC_2T_x$ film (9 nm thick) were measured to be 0.00015 ± 0.00001 Ohm·cm and 0.0062 ± 0.0013 Ohm·cm, respectively (**Table S3)**. We note that optical resistivity calculated based on the SE data represents that of an effective medium approximation, where the path length of light can depend on both the surface coverage of the MXene flakes as well as the film thickness.[35, 69, 70] As such, the resistivity of the material appears to be smaller in thinner MXene films. A similar effect can be observed in thin films of gold if the film thickness is such that a full extinction of light is not achieved (**Figure S12**). To obtain the corresponding value of resistivity from the optical resistivity calculations, one needs to perform measurements on much thicker and denser films, where the measured complex index of refraction eventually reaches a plateau value. As a result, the optical resistivity values reported here represent a lower boundary value of the DC resistivity but are expected to be within the same order of magnitude as the true value.

Thermal degradation of MXenes under ambient conditions. To investigate the degree of oxidation and thermal stability of the $Ti_3C_2T_x$ MXene, in-situ SE was performed while the sample was heated up to 600 °C in ambient conditions, with a controlled rate of 10 °C/min (schematically shown in **Figure 1c**, more details in the Materials and Methods section). We note that once the MXene is degraded and conductivity reaches zero, the resistivity value diverges and becomes inaccurate, as such a more limited range of data is presented here. **Figure 3a** shows the evolution of the optical absorption spectra for a 9-nm-thick $Ti_3C_2T_x$ film at various temperatures upon heating. As the MXene film is thermally degraded, the extinction amplitude decreases, indicating the loss of conductivity as well as the formation of TiO_2, which is transparent in the visible and near-IR optical region, explored in this study. **Figures 3b-d** show the in-situ variations of the optical resistivity as well as the extinction wavelength and amplitude of the harmonic 2 oscillator as a function of temperature. The data is compared with TGA mass loss, under similar conditions as reported previously.[22]

A few distinct trends can be noted in this data. Heating the $Ti_3C_2T_x$ from room temperature to 100 °C, has minimal effect on conductivity (highlighted in the inset of **Figure 3b**), while resulting in red-shifting of the extinction peak (**Figure 3c**). The TGA data (black curve in **Figure 3b**) also shows little to no weight loss up to 100 °C. We interpret these observations as indicating that while some water molecules may evaporate from the free surface, most water molecules adsorbed on MXene surfaces, particularly in the inter-flake slits remain intact. In addition to resistivity, the dielectric constant of the film and thus its extinction spectrum remains nearly the same between 25 °C – 100 °C (**Figure 3a**). If the harmonic 2 oscillator had a plasmonic origin,

we would expect the plasmon resonance to either remain constant or slightly blue-shift due to lower local index of refraction of adsorbed water (dielectric).[58] However, the data in **Figure 3c** shows a strong red-shifting of the extinction peak energy. This is likely due to the intrinsic temperature dependence of the corresponding inter-band transition, which should be further explored in properly dried MXene samples in the future. In addition, changes in the oxidation state of the Ti in $Ti_3C_2T_x$ upon heating can cause red-shifting of the extinction peak energy.[22, 36]

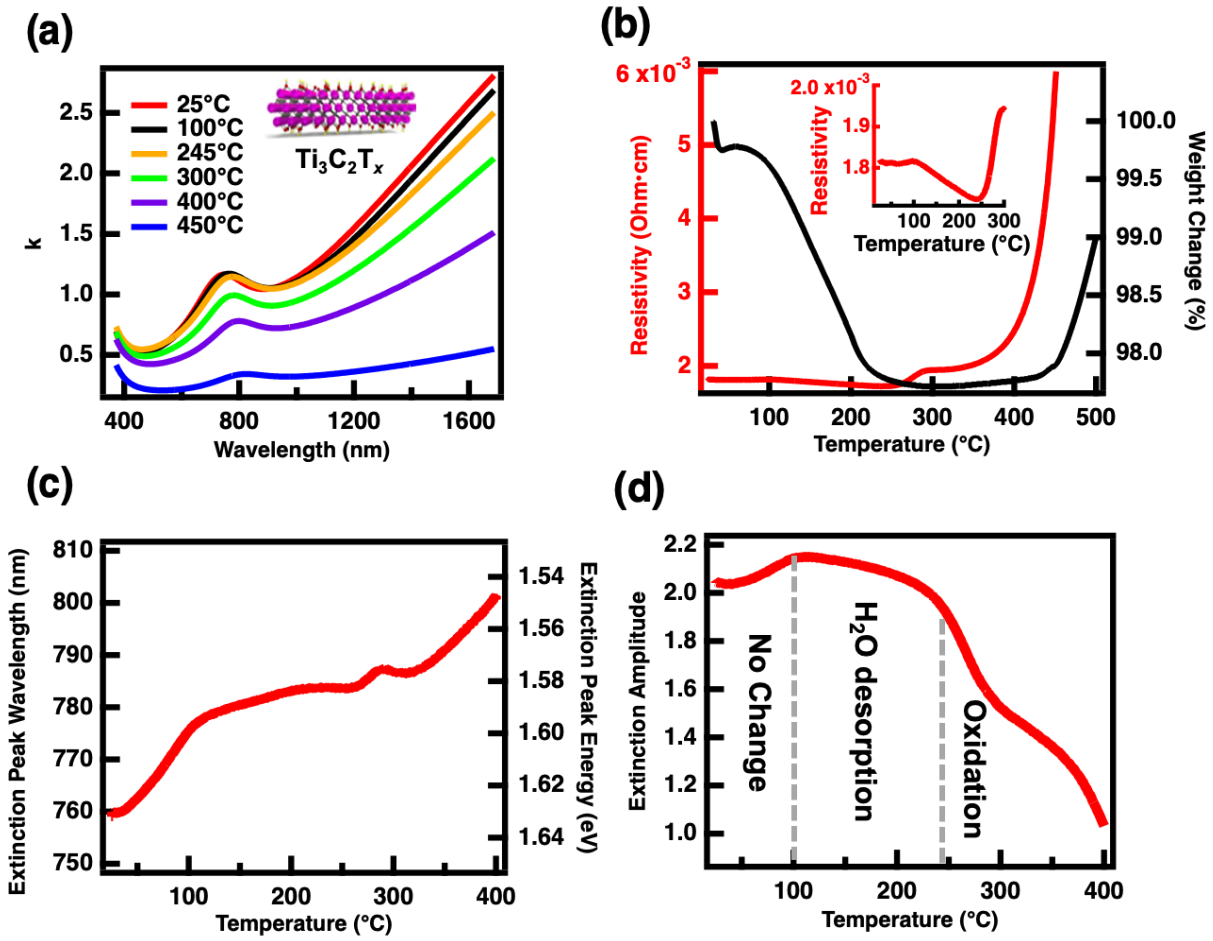

Figure 3. (a) The imaginary part of the index of refraction, k, for a 19 nm $Ti_3C_2T_x$ film measured at various temperatures upon in-situ heating in air at 10 °C/min. **(b)** Optical resistivity measured using SE and weight change measured using TGA as a function of temperature upon heating at a rate of 10 °C/min. The inset shows the details of change in the optical resistivity due to the desorption of surface-adsorbed water, before the onset of degradation. **(c** and **d)** the extinction peak wavelength and amplitude for the harmonic 2 oscillator as a function of temperature.

As the heating continues from 100 °C to 245 °C, the film's resistivity decreases (highlighted in the inset of **Figure 3b**) in conjunction with weight loss observed in TGA (black curve, **Figure 3b**), indicating the desorption of H_2O in this temperature range. The desorption of

water, and higher energy of the remaining water molecules can reduce the contact resistance between the flakes, resulting in the observed increased conductivity and reduced resistivity. We also observe that in this temperature range, both the amplitude and the energy of the harmonic 2 oscillator are relatively constant, with only a small degree of red-shifting in the extinction energy. This is likely due to an interplay between the intrinsic red-shifting seen at lower temperatures, and the removal of water, which significantly changes the local dielectric constant of the interfacial region. Loss of –OH and formation of =O terminations, leading to an increase in the oxidation state of Ti is known to redshift this absorption peak. However, we again note that a plasmonic origin would predict blue-shifting of this resonance upon heating. The decrease in resistivity upon H_2O removal is in line with previously reported in-situ TEM results, where the electronic resistivity decreased with increasing the annealing temperature.[39] In addition, DFT calculations have predicted that the de-functionalization of $Ti_3C_2T_x$ surface can increase its density of states (DOS) at the Fermi level (EF), which can intensify the charge carrier density, and thus enhance the conductivity.[39, 71] As a result, the redshift of the plasmon peak can be also ascribed to growing metallic-like free electron density caused by the surface group de-functionalization or the de-intercalation of the H_2O molecules. This is also consistent with the slight enhancement in the plasmon amplitude below 100 °C (**Figure 3d**). The small change in the overall spectrum of the MXene films in this temperature range indicates that despite the H_2O removal, $Ti_3C_2T_x$ MXene does not significantly degrade upon heating to 245 °C under ambient conditions. Previous measurements using nuclear magnetic resonance and neutron scattering showed high stability of surface hydroxyl groups below 230 °C,[72, 73] which is consistent with these observations. As such, annealing in this temperature range, even in ambient conditions, can be used as an effective method to tailor the conductivity and NIR spectral properties of $Ti_3C_2T_x$ MXene, which are important in various applications.

When the temperature is increased further to above 245 °C in air, the extinction coefficient of the film decreases and the resistivity increases (**Figures 3a, b, and d**). This is evidence of more significant changes in the MXene composition upon thermal annealing and the eventual onset of degradation. This observation is consistent with previous TGA measurements[22] as well as the TGA data shown in **Figure 3b** that indicates MXene degradation. Monotonous decrease of the extinction coefficient and the amplitude of the harmonic 2 oscillator can be interpreted as a combination of the reduction of the number and the mass of MXene flakes,[74] the changing nature of its surface terminations[40, 75], and finally MXene oxidation to form TiO_2 nanocrystals and disordered carbon, which are transparent.[22] This is corroborated by the TGA data that shows an overall weight loss of the material reaching a minimum at 300 °C (black line, **Figure 3b**). This

weight loss indicates the start of the removal of surface –OH groups and removal of the remaining H_2O, while the increase in the mass at higher temperatures indicates the oxygen uptake and formation of oxides. These results are consistent with the previously reported $Ti_3C_2T_x$ MXene TGA data that a gradual weight loss was observed from room temperature to about 400 °C when measurements were performed in vacuum.[45,50, 74] Continuing heating to above 450 °C, we observe a rapid onset in increased resistivity, strong decrease in extinction, and the harmonic 2 oscillator amplitude, along with a weight increase in the TGA results. These trends can be attributed to the formation of transparent metal oxides (*e.g.*, TiO_2) upon the oxidation reaction in air.[45, 46]

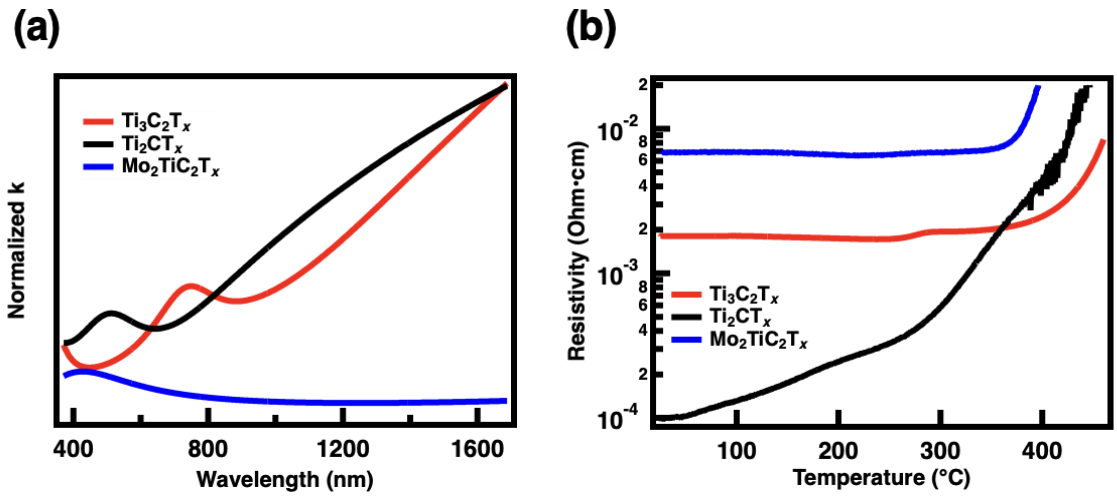

Figure 4. (a) Normalized extinction coefficients (normalized k) of $Ti_3C_2T_x$ (19 nm film, red curve), Ti_2CT_x (3 nm film, black curve), and $Mo_2TiC_2T_x$ (9 nm, blue curve) MXene films measured at room temperature. **(b)** The deduced optical resistivity of these MXene films as a function of temperature, measured upon heating with a rate of 10 °C/min.

The combination of trends observed in the resistivity and extinction properties of $Ti_3C_2T_x$ MXene indicates that in-situ SE measurements can capture indirect information on the changes in MXene surface terminations at low temperatures as well as the onset and details of the degradation rate at higher temperatures. The advantage of these measurements over TGA data is that this method can be applied to MXene films with various thicknesses and on various substrates, allowing precise tailoring of the optical properties to the desired conditions, without fully destroying the sample. In addition, these measurements can be extended in the future to experiments under various environmental conditions and under isothermal annealing, which can be used to measure the rates and apparent activation energy for adsorption-desorption and degradation reactions.

These measurements can also be extended to various MXene types to study their relative thermal stability. An example is shown in **Figure 4**, where we compare the normalized extinction coefficient, measured through k (**Figure 4a**), and the temperature-dependent resistivity (**Figure 4g**) of Ti_2CT_x and $Mo_2TiC_2T_x$ with $Ti_3C_2T_x$ MXene. The details of fitting procedures and results can be found in SI and **Table S3**, as well as **Figures S8-11**. Ti_2CT_x, which consists of the similar M and X elements (Ti and C) as to $Ti_3C_2T_x$ but with a smaller thickness, has a qualitatively similar extinction spectrum at room temperature, but with a red-shifted extinction peak (**Figure 4a**). This is consistent with previous DFT predictions as detailed in the previous section.[71] Previous studies also indicate that in bulk films, $Ti_3C_2T_x$ and Ti_2CT_x have similar DC conductivity and carrier concentrations as high as 3×10^{22} cm^{-3}.[10, 76, 77] As such, the difference between the initial values of optical resistivity seen in **Figure 4** can be mainly attributed to the differences in their initial film thickness (19 nm for $Ti_3C_2T_x$ film vs. 3 nm for Ti_2CT_x film). As discussed earlier, a higher apparent optical conductivity (lower optical resistivity) is expected in thinner films, due to the shorter optical pathlength through these samples.

When heated above room temperature in ambient conditions, the resistivity of Ti_2CT_x increases slowly until 300 °C (**Figure 4b**). This contrasts with measurements in $Ti_3C_2T_x$, where the removal of surface water resulted in decreasing conductivity at elevated temperatures. To understand this data, we note that the 3-nm-thick Ti_2CT_x film in this study is primarily composed of few MXene flakes and as such, the measured conductivity here is reflective of its intrinsic intra-flake conductivity as opposed to carrier transport through the inter-flake regions, which should dominate our measurements in thicker films, such as in the 19-nm-thick $Ti_3C_2T_x$ film. Given the metallic nature of this MXene, we expect a positive temperature-dependent resistivity ($dR/dT>0$)[39, 78] This may also partially explain the lower value of resistivity in this system. Similar measurements in $Ti_3C_2T_x$ single-flake films in the future can verify whether a similar temperature dependence can be observed in this system. When heating is continued to above 300 °C, we see a more dramatic increase in resistivity (**Figure 4b**), which is also followed by a sudden blue-shifting of the harmonic 2 extinction energy and a decrease in its amplitude (**Figures S8a&b**). This is an indication of the onset of oxidation in Ti_2CT_x, consistent with TGA measurements shown in **Figure S5**. Compared to $Ti_3C_2T_x$ (oxidation onset at 450 °C) this MXene is thermally less stable, as has been reported previously.[79]

The replacement of the outer layers Ti atoms with Mo in $Mo_2TiC_2T_x$ MXene has a more dramatic effect on the extinction spectrum. The SE data for this MXene can mostly be fitted using only one harmonic oscillator, with the interband transition at 2.6 eV (470 nm). The optical

conductivity of the sample and overall extinction is also lower than that of $Ti_3C_2T_x$ despite the fact that these measurements were performed in a thinner film (9-nm-thick film for $Mo_2TiC_2T_x$ and 14-nm-thick film for $Ti_3C_2T_x$), indicating that the bulk DC conductivity of $Mo_2TiC_2T_x$ is also lower than that of $Ti_3C_2T_x$. While some previous studies had indicated an intrinsic metallic nature in $Mo_2TiC_2T_x$ [39, 41] they observe a much lower carrier concentration compared to $Ti_3C_2T_x$, in the range of 2-8 × 10^{20} cm^{-3}.[80] In contrast, DFT calculations have predicted semiconducting behavior as opposed to metallic properties, with a small bandgap of 0.05 eV.[68] To investigate whether the properties can be described by a semiconductor, an alternative fitting procedure was used where the Drude oscillator was replaced by a Gaussian fit, which provides a bandgap of 0.06 eV (**Figure S11** with more details provided in SI), consistent with these predictions. Within the limited optical window of our experiments, both Drude and Gaussian oscillators fit the data equally well. As such, to distinguish this difference, measurements need to be extended into the IR spectral region. We also note that given the rather small bandgap, synthetic details, such as the number of defects and surface terminations, can affect the carrier concentrations at the Fermi level, allowing this MXene to have either metallic or semiconducting properties. In this study $Mo_2TiC_2T_x$ is intercalated with TMA^+, which is a large organic ion and can significantly increase the inter-flake spacing and electrical resistance,[66] leading to higher optical resistivity than it may be possible otherwise.

Nevertheless, we can compare the optical resistivity of $Mo_2TiC_2T_x$ with $Ti_3C_2T_x$ as a function of temperature, to compare their thermal stability. We note that, if a Gaussian model is used instead of the Drude oscillator for $Mo_2TiC_2T_x$, the conclusions regarding thermal stability, measured through measurements of the bandgap and its amplitude as a function of temperature, remain the same (more details SI and **Figures S11c, d**). The trends in optical properties of the two MXenes are very similar. However, the onset of oxidation is lower in $Mo_2TiC_2T_x$ and is observed at 400 °C (**Figures 4b, S8a,** and **S8b**). This is likely due to the stronger Ti-Ti bonding relative to Mo-Ti bonding, which protects the surface terminations to a higher temperature.[39, 41] Additionally, the harsher synthesis conditions, etching with 50% HF and delamination with TMAOH that was needed for the synthesis of $Mo_2TiC_2T_x$ lead to a greater number of defects and smaller flake sizes.

Overall, the measurements of thermal evolution of MXenes through changes in optical properties, measured using in-situ SE, provide information complementing TGA measurements. However, these measurements are performed in the thin film condition, where single-flake level properties can be explored, as shown for Ti_2CT_x. For all studied MXenes, the two distinct peaks observed in MS spectra (**Figures S5&S6** for Ti_2CT_x and $Mo_2TiC_2T_x$, and reference [39] for $Ti_3C_2T_x$)

centered at around 100-200 °C can be assigned to the removal of surface adsorbed and intercalated H_2O molecules (mass to charge ratio (m/z) =18) as well as de-functionalization of the –OH terminations (mass to charge ratio (m/z) =17). This trend was observed as decreasing resistivity in thicker MXene films ($Ti_3C_2T_x$ and $Mo_2TiC_2T_x$) and increasing resistivity in 3-nm films (Ti_2CT_x). Heating in ambient environment to elevated temperatures, where a mass increase was observed in TGA-MS measurements due to oxidation (**Figure 3b** for $Ti_3C_2T_x$ and **Figures S5&S6** for Ti_2CT_x and $Mo_2TiC_2T_x$, and reference [39] for Ti_3C_2), was also evident in in-situ SE measurements as a sudden onset of increased resistivity (**Figure 4b**) in all MXenes. The degradation temperature was measured at 300 °C, 400 °C, and 450 °C for Ti_2CT_x, $Mo_2TiC_2T_x$ and $Ti_3C_2T_x$, respectively, indicating the increasing trend in the thermal stability of these three MXenes. As such, in-situ SE represents a rapid, non-destructive, and accurate approach to measure both, the optical conductivity and thermal stability of MXene films, which can be used in the future to explore the thickness dependence of these properties, as well as the utilization of various methods in improving both conductivity and stability of a broad range of MXenes.

Conclusions

In this work, we conducted in-situ spectroscopic ellipsometry to study the optical properties and thermal stability of MXenes upon heating in air. In multilayer MXene films, moderate heating above room temperature resulted in the removal of surface adsorbed and intercalated water and –OH terminations, which improved MXene electrical conductivity. Further heating led to the onset of thermal oxidation, as indicated by a dramatic increase in resistivity. The oxidation onset temperatures follows the sequence of $Ti_3C_2T_x$ > $Mo_2TiC_2T_x$ > Ti_2CT_x; the reduction of atomic layer thickness and replacement of Ti with Mo both lower thermal stability. The results indicate a strong dependency of the thermal properties on the chemical composition including the type of transition metal, the atomic structure, and the surface chemistry, as well as 2D flake quality. Our results also indicate that annealing below the oxidation temperature is an effective, simple, and scalable approach to tune the optical properties and enhance conductivity of MXenes. Although this work highlights the promise of spectroscopic ellipsometry for correlating optical properties of MXenes with their surface functionality and monitoring MXenes oxidation in a non-destructive way, a combination of theoretical and experimental insights can help further expand knowledge about optical properties of MXenes.

Materials and Methods

Materials. Frosted glass substrates were purchased from Fisher Scientific. Ti (99.5%, -325 mesh), Mo (99.5%, -325 mesh), Al (99.5%, -325 mesh), TiC (99.5%, 2 μm), C (graphite, 99.0%, -325 mesh) powders were supplied from Alfa Aesar. Argon (Ar) (99.995%) gas was purchased from Air Gas. HF (48.5-51%, Acros Organics), HCl (36.5-38%, Fisher Chemical), LiCl (99%, Acros Organics), and TMAOH (25 wt %, Acros Organics) were used as received.

MAX synthesis. For each MAX phase, precursors were mixed in the powder form with different ratios (**Table S1**). Then, 10 mm zirconia balls were added to each mixed powder in a 2:1 ball/powder ratio. The mixtures were transferred into plastic jars, followed by ball milling at 50 rpm for 18 h. The uniform powder blends were then placed into alumina pots and placed in an air-free furnace (Carbolite Gero) continuously purged with Ar, heated at a heating rate of 3 °C min^{-1}. MAX phases were formed at specific temperatures and holding times as detailed in **Table S1**. After cooling, a TiN-coated milling bit was used to mill the obtained MAX phases[22, 81], followed by sieving each sample to less than 75 μm particle size.

MXene synthesis. $Ti_3C_2T_x$ and Ti_2CT_x were synthesized by selective etching of aluminum from their corresponding MAX phases (Ti_3AlC_2 and Ti_2AlC) with a mixture solution of HF and HCl.[65, 82] Typically, 2 mL of HF, 12 mL of HCl, and 6 mL of deionized (DI) water were mixed. After that, 1 g of each MAX phase powder was added to the solution and stirred for 24 h at 35 ºC. After etching, the reaction products were washed with DI water and centrifuged at 3500 rpm for 2 mins until the pH was greater than 6. The obtained sediments were dispersed in a 0.5 M LiCl solution. The mixtures were stirred for 4 h at 35 ºC, and then centrifuged at 3500 rpm for 10 mins several times until the sediments turned to black. The swelled sediments were dispersed in DI water and then centrifuged at 3500 rpm for 10 mins. Finally, the dark supernatants were collected for characterization. Different with the $Ti_3C_2T_x$ used for in-situ spectroscopic ellipsometry measurements (Figure 3), an optimized $Ti_3C_2T_x$ was used for the multi-angle spectroscopic ellipsometry measurements (Figure 2). The details about the new developed optimized $Ti_3C_2T_x$ can be found in the 2023 article.[27]

$Mo_2TiC_2T_x$ was synthesized by selective etching of Mo_2TiAlC_2 MAX phase powder using HF.[65] Typically, 1 g of MAX phase powder was added to 20 mL of an HF solution followed by stirring at 50 °C for 48 h. After the etching step, the resulting solution was washed with DI water through centrifugation (3500 rpm, 2 min) several times, until the pH value was greater than 6. Then, the centrifuged sediment was added into a solution containing 1 g of TMAOH and 20 mL

of DI water and stirred for 12 h at room temperature. The mixture was centrifuged several times with DI water at 9000 rpm for 10 min until the pH value was less than 8. Finally, the solution was centrifuged at 3500 rpm for 10 min. The black supernatant was taken as the dispersion of delaminated MXene flakes in water.

Fabrication of MXenes Films. For SE measurements, frosted glass substrates were cleaved into approximately 1cm × 1cm squares and were cleaned with toluene and ethanol several times before being exposed to oxygen plasma for 2 min. After plasma treatment, glass substrates were rinsed in methanol. Colloidal MXenes solutions were used for spin-coating. The concentration of colloidal solution for $Ti_3C_2T_x$, Ti_2CT_x and $Mo_2TiC_2T_x$ were 5-7 mg/mL, 0.5 mg/mL, and 5 mg/mL, respectively. All colloidal solutions were bath-sonicated for 15 min before spin-coating. MXene films were constructed on the frosted glasses via a two-step spin coating (Laurell WS 400BZ-6NPP/Lite spin-coater) at 500-1000 rpm for 30 s followed by 5 s at 750-1250 rpm. Spin-coated films were vacuum dried at 50 °C/min for 30 min, followed by air-drying at 80 °C/min on a 22 mm temperature-controlled stage (Linkam THMS 600) with 10 °C/min heating and cooling ramps.

To perform XRD and TGA-MS experiments, free-standing films of the three MXenes were prepared by vacuum-assisted filtration of the delaminated single-layer MXene colloidal solutions on Celgard®3501 membrane filters. The films were dried and kept under vacuum at room temperature in a desiccator before characterization.

Characterization Methods

X-ray diffraction measurements. XRD patterns were collected at room temperature using an X-ray diffractometer (Rigaku SmartLab) equipped with a Cu K_α radiation source with the wavelength of λ= 1.5418 Å working at 20 mA and 40 kV. The results are shown in **Figures S1&S3**.

Field-emission scanning electron microscopy (FESEM). (FESEM) was performed using a JEOL JSM-7800f FESEM with a lower electron detector at an acceleration voltage of 5 kV and 15 kV to study the morphology of the optimized-Ti_3AlC_2 MAX and $Ti_3C_2T_x$ MXene, respectively. The optimized-Ti_3AlC_2 MAX particles were sieved using mesh size < 71 μm and loaded on carbon tape. The $Ti_3C_2T_x$ MXene solution concentration was maintained at < 0.1 mg $mL^{-}1$ and loaded on an anodic disc, followed by vacuum drying for 2 h. The samples were gold sputtered to reduce the charging and improve the sharpness of SEM images. Image J software was used to calculate the average flake size from the FESEM images. The images are shown in **Figures S2&S4**

Thermogravimetric analysis. A TA Instruments thermal analyzer (SDT Q 650, Discovery Series) equipped with a mass spectrometer (MS, 110/220V) was used to perform TGA-MS analysis of Ti_2CT_x and $Mo_2TiC_2T_x$ MXenes (**Figures S5&S6**, respectively). For $Ti_3C_2T_x$ MXene, data from previous literature was used.[22, 83] TGA-MS thermograms were collected from room temperature to 600 °C with a ramp rate of 10 ºC/min under 100 mL/min air flow. Mass/charge (m/z) evolution profiles were recorded as a function of temperature by MS analysis of the evolved gas products. The ion current was normalized by the corresponding initial weight of material. A quadrupole detection system, including a closed ion source, triple mass filter, and dual (Faraday and Secondary Electron Multiplier) detector provided parts per billion (ppb) sensitivity over the mass range of 1-300 amu (atomic mass unit; gas dependent).

Atomic Force Microscopy (AFM). Morphology of the deposited Ti_3C_2Tx film was measured using a Bruker Icon AFM (Bruker, Santa Barbara CA) AFM in tapping mode. The tapping mode AFM probe with aluminum reflective coating (Budget Sensors, Tap300Al-G, resonance frequency 300 kHz, tip radius 10 nm) probe was used. Images were obtained with a resolution of 256 by 256 pixel and were analyzed using Gwyddion software. The images are shown in **Figures S7.**

Spectroscopic ellipsometry. SE measurements were performed using a Woollam M-2000 ellipsometer (J.A. Woollam) with a wavelength range of 370 nm < λ < 1600 nm (0.73 eV – 3.34 eV). The optical spectra of as-prepared $Ti_3C_2T_x$ were collected using variable angle measurements (**Figure 2** and **Table S2**). For in-situ experiments, of all three MXenes the incident angle was fixed at 70 ° (**Figures S8-S11** and **Table S3**). After drying MXenes films, the samples were clamped onto the Linkam heating stage and placed under the ellipsometer. The thermal annealing of MXene films was performed in the temperature range of 25 °C to 600 °C under air at a heating rate of 10 °C/min, while the SE spectra were collected. The desired temperatures and heating rates were controlled by the Linksys software. The sampling rate for in-situ SE measurements was set at 1 sec, with high accuracy zone averaging. Details of SE data analysis and fitting models can be found in the SI. The fitting results for the variable-angle SE measurements of $Ti_3C_2T_x$ are listed in **Table S2** and the data obtained at the beginning of in-situ experiments at room temperature are listed in **Table S3.** We note that the slight difference in values for $Ti_3C_2T_x$ are because different batches of samples were used for these measurements, with slight variability in flake size and properties.

Author Contributions

A.A.S., A.T., and D.Z. conducted synthesis; A.A.S. and D.Z. conducted XRD and TGA characterization; A.A.S. and H.F. conducted ellipsometry characterization with the help of Y.C., A.X., and H.W.; H.F. performed ellipsometry data analysis. A.A.S. and H.F. prepared the first draft of the manuscript. Y.G. and Z.F. conceptualized the study and B.A., M.S. Y.G. and Z.F. supervised the study and edited the manuscript. The manuscript was written through contributions of all authors and all authors have given approval to the final version of the manuscript.

Notes

The authors declare no competing financial interest.

Acknowledgments

This work was primarily supported by the National Science Foundation (NSF) Future Manufacturing Research Grant (CMMI-2134607). A.A.S. was supported with a postdoctoral fellowship from the Vagelos Institute of Energy Science and Technology (VIEST). Y.C. acknowledges support from the NSF Graduate Research Fellowship Program (NSF GRFP, DGE-1845298), and H.F. acknowledges postdoctoral fellowship funding from the School of Arts and Sciences at the University of Pennsylvania. D.Z. and Y.G. acknowledge funding from NSF grant DMR-2041050 for MXene synthesis performed at Drexel University.

References

1. Hantanasirisakul, K.; Gogotsi, Y., Electronic and optical properties of 2D transition metal carbides and nitrides (MXenes). *Advanced Materials* **2018,** *30* (52), 1804779.
2. Gogotsi, Y.; Anasori, B., The rise of MXenes. ACS Publications: 2019; Vol. 13, pp 8491-8494.
3. Zhang, D.; Shah, D.; Boltasseva, A.; Gogotsi, Y., MXenes for photonics. *ACS Photonics* **2022,** *9* (4), 1108-1116.
4. Anasori, B.; Gogotsi, Û. G., *2D metal carbides and nitrides (MXenes)*. Springer: 2019; Vol. 2549.
5. Luo, J.; Tao, X.; Zhang, J.; Xia, Y.; Huang, H.; Zhang, L.; Gan, Y.; Liang, C.; Zhang, W., Sn4+ ion decorated highly conductive Ti3C2 MXene: promising lithium-ion anodes with enhanced volumetric capacity and cyclic performance. *ACS nano* **2016,** *10* (2), 2491-2499.
6. Lukatskaya, M. R.; Kota, S.; Lin, Z.; Zhao, M.-Q.; Shpigel, N.; Levi, M. D.; Halim, J.; Taberna, P.-L.; Barsoum, M. W.; Simon, P., Ultra-high-rate pseudocapacitive energy storage in two-dimensional transition metal carbides. *Nature Energy* **2017,** *2* (8), 1-6.
7. Ghidiu, M.; Lukatskaya, M. R.; Zhao, M.-Q.; Gogotsi, Y.; Barsoum, M. W., Conductive two-dimensional titanium carbide 'clay'with high volumetric capacitance. *Nature* **2014,** *516* (7529), 78-81.
8. Liu, Y. T.; Zhang, P.; Sun, N.; Anasori, B.; Zhu, Q. Z.; Liu, H.; Gogotsi, Y.; Xu, B., Self-assembly of transition metal oxide nanostructures on MXene nanosheets for fast and stable lithium storage. *Advanced Materials* **2018,** *30* (23), 1707334.
9. Hantanasirisakul, K.; Zhao, M. Q.; Urbankowski, P.; Halim, J.; Anasori, B.; Kota, S.; Ren, C. E.; Barsoum, M. W.; Gogotsi, Y., Fabrication of Ti3C2Tx MXene transparent thin films with tunable optoelectronic properties. *Advanced Electronic Materials* **2016,** *2* (6), 1600050.
10. Dillon, A. D.; Ghidiu, M. J.; Krick, A. L.; Griggs, J.; May, S. J.; Gogotsi, Y.; Barsoum, M. W.; Fafarman, A. T., Highly conductive optical quality solution-processed films of 2D titanium carbide. *Advanced Functional Materials* **2016,** *26* (23), 4162-4168.
11. Ying, G.; Dillon, A. D.; Fafarman, A. T.; Barsoum, M. W., Transparent, conductive solution processed spincast 2D Ti2CT x (MXene) films. *Materials Research Letters* **2017,** *5* (6), 391-398.
12. Yu, X.-f.; Li, Y.-c.; Cheng, J.-b.; Liu, Z.-b.; Li, Q.-z.; Li, W.-z.; Yang, X.; Xiao, B., Monolayer Ti2CO2: a promising candidate for NH3 sensor or capturer with high sensitivity and selectivity. *ACS applied materials & interfaces* **2015,** *7* (24), 13707-13713.
13. Kim, S. J.; Koh, H.-J.; Ren, C. E.; Kwon, O.; Maleski, K.; Cho, S.-Y.; Anasori, B.; Kim, C.-K.; Choi, Y.-K.; Kim, J., Metallic Ti3C2T x MXene gas sensors with ultrahigh signal-to-noise ratio. *ACS nano* **2018,** *12* (2), 986-993.
14. Lee, E.; VahidMohammadi, A.; Prorok, B. C.; Yoon, Y. S.; Beidaghi, M.; Kim, D.-J., Room temperature gas sensing of two-dimensional titanium carbide (MXene). *ACS applied materials & interfaces* **2017,** *9* (42), 37184-37190.
15. Sarycheva, A.; Polemi, A.; Liu, Y.; Dandekar, K.; Anasori, B.; Gogotsi, Y., 2D titanium carbide (MXene) for wireless communication. *Science advances* **2018,** *4* (9), eaau0920.
16. Gao, G.; O'Mullane, A. P.; Du, A., 2D MXenes: a new family of promising catalysts for the hydrogen evolution reaction. *Acs Catalysis* **2017,** *7* (1), 494-500.
17. Levitt, A.; Zhang, J.; Dion, G.; Gogotsi, Y.; Razal, J. M., MXene-based fibers, yarns, and fabrics for wearable energy storage devices. *Advanced Functional Materials* **2020,** *30* (47), 2000739.
18. Anasori, B.; Lukatskaya, M. R.; Gogotsi, Y., 2D metal carbides and nitrides (MXenes) for energy storage. *Nature Reviews Materials* **2017,** *2* (2), 1-17.
19. Naguib, M.; Kurtoglu, M.; Presser, V.; Lu, J.; Niu, J.; Heon, M.; Hultman, L.; Gogotsi, Y.; Barsoum, M. W., Two-dimensional nanocrystals produced by exfoliation of Ti3AlC2. *Advanced materials* **2011,** *23* (37), 4248-4253.

20. Verger, L.; Xu, C.; Natu, V.; Cheng, H.-M.; Ren, W.; Barsoum, M. W., Overview of the synthesis of MXenes and other ultrathin 2D transition metal carbides and nitrides. *Current Opinion in Solid State and Materials Science* **2019,** *23* (3), 149-163.
21. Lim, K. R. G.; Shekhirev, M.; Wyatt, B. C.; Anasori, B.; Gogotsi, Y.; Seh, Z. W., Fundamentals of MXene synthesis. *Nature Synthesis* **2022,** *1* (8), 601-614.
22. Mathis, T. S.; Maleski, K.; Goad, A.; Sarycheva, A.; Anayee, M.; Foucher, A. C.; Hantanasirisakul, K.; Shuck, C. E.; Stach, E. A.; Gogotsi, Y., Modified MAX phase synthesis for environmentally stable and highly conductive Ti3C2 MXene. *ACS nano* **2021,** *15* (4), 6420-6429.
23. Anayee, M.; Shuck, C. E.; Shekhirev, M.; Goad, A.; Wang, R.; Gogotsi, Y., Kinetics of Ti3AlC2 Etching for Ti3C2T x MXene Synthesis. *Chemistry of Materials* **2022,** *34* (21), 9589-9600.
24. Alhabeb, M.; Maleski, K.; Anasori, B.; Lelyukh, P.; Clark, L.; Sin, S.; Gogotsi, Y., Guidelines for synthesis and processing of two-dimensional titanium carbide (Ti3C2T x MXene). *Chemistry of Materials* **2017,** *29* (18), 7633-7644.
25. Michałowski, P. P.; Anayee, M.; Mathis, T. S.; Kozdra, S.; Wójcik, A.; Hantanasirisakul, K.; Jóźwik, I.; Piątkowska, A.; Możdżonek, M.; Malinowska, A., Oxycarbide MXenes and MAX phases identification using monoatomic layer-by-layer analysis with ultralow-energy secondary-ion mass spectrometry. *Nature Nanotechnology* **2022,** *17* (11), 1192-1197.
26. Shekhirev, M.; Ogawa, Y.; Shuck, C. E.; Anayee, M.; Torita, T.; Gogotsi, Y., Delamination of Ti3C2T x Nanosheets with NaCl and KCl for Improved Environmental Stability of MXene Films. *ACS Applied Nano Materials* **2022,** *5* (11), 16027-16032.
27. Thakur, A.; Chandran BS, N.; Davidson, K.; Bedford, A.; Fang, H.; Im, Y.; Kanduri, V.; Wyatt, B. C.; Nemani, S. K.; Poliukhova, V., Step-by-Step Guide for Synthesis and Delamination of Ti3C2Tx MXene. *Small Methods* **2023**, 2300030.
28. Li, G.; Kushnir, K.; Dong, Y.; Chertopalov, S.; Rao, A. M.; Mochalin, V. N.; Podila, R.; Titova, L. V., Equilibrium and non-equilibrium free carrier dynamics in 2D Ti3C2Tx MXenes: THz spectroscopy study. *2D Materials* **2018,** *5* (3), 035043.
29. Xu, X.; Guo, T.; Lanza, M.; Alshareef, H. N., Status and prospects of MXene-based nanoelectronic devices. *Matter* **2023**.
30. Mauchamp, V.; Bugnet, M.; Bellido, E. P.; Botton, G. A.; Moreau, P.; Magne, D.; Naguib, M.; Cabioc'h, T.; Barsoum, M. W., Enhanced and tunable surface plasmons in two-dimensional Ti 3 C 2 stacks: Electronic structure versus boundary effects. *Physical Review B* **2014,** *89* (23), 235428.
31. El-Demellawi, J. K.; Lopatin, S.; Yin, J.; Mohammed, O. F.; Alshareef, H. N., Tunable Multipolar Surface Plasmons in 2D Ti3C2 T x MXene Flakes. *ACS nano* **2018,** *12* (8), 8485-8493.
32. Maleski, K.; Shuck, C. E.; Fafarman, A. T.; Gogotsi, Y., The broad chromatic range of two-dimensional transition metal carbides. *Advanced Optical Materials* **2021,** *9* (4), 2001563.
33. Lashgari, H.; Abolhassani, M.; Boochani, A.; Elahi, S.; Khodadadi, J., Electronic and optical properties of 2D graphene-like compounds titanium carbides and nitrides: DFT calculations. *Solid state communications* **2014,** *195*, 61-69.
34. Magne, D.; Mauchamp, V.; Célérier, S.; Chartier, P.; Cabioc'h, T., Spectroscopic evidence in the visible-ultraviolet energy range of surface functionalization sites in the multilayer Ti 3 C 2 MXene. *Physical Review B* **2015,** *91* (20), 201409.
35. Lioi, D. B.; Stevenson, P. R.; Seymour, B. T.; Neher, G.; Schaller, R. D.; Gosztola, D. J.; Vaia, R. A.; Vernon, J. P.; Kennedy, W. J., Simultaneous Ultrafast Transmission and Reflection of Nanometer-Thick Ti3C2T x MXene Films in the Visible and Near-Infrared: Implications for Energy Storage, Electromagnetic Shielding, and Laser Systems. *ACS Applied Nano Materials* **2020,** *3* (10), 9604-9609.
36. Salles, P.; Pinto, D.; Hantanasirisakul, K.; Maleski, K.; Shuck, C. E.; Gogotsi, Y., Electrochromic effect in titanium carbide MXene thin films produced by dip-coating. *Advanced Functional Materials* **2019,** *29* (17), 1809223.

37. Zhang, D.; Wang, R.; Wang, X.; Gogotsi, Y., In situ monitoring redox processes in energy storage using UV–Vis spectroscopy. *Nature Energy* **2023**, 1-10.
38. Bai, Y.; Zhou, K.; Srikanth, N.; Pang, J. H.; He, X.; Wang, R., Dependence of elastic and optical properties on surface terminated groups in two-dimensional MXene monolayers: a first-principles study. *RSC advances* **2016,** *6* (42), 35731-35739.
39. Hart, J. L.; Hantanasirisakul, K.; Lang, A. C.; Anasori, B.; Pinto, D.; Pivak, Y.; van Omme, J. T.; May, S. J.; Gogotsi, Y.; Taheri, M. L., Control of MXenes' electronic properties through termination and intercalation. *Nature communications* **2019,** *10* (1), 522.
40. Hart, J. L.; Hantanasirisakul, K.; Lang, A. C.; Li, Y.; Mehmood, F.; Pachter, R.; Frenkel, A. I.; Gogotsi, Y.; Taheri, M. L., Multimodal spectroscopic study of surface termination evolution in Cr2TiC2Tx MXene. *Advanced Materials Interfaces* **2021,** *8* (5), 2001789.
41. Hart, J. L.; Hantanasirisakul, K.; Gogotsi, Y.; Taheri, M. L., Termination-property coupling via reversible oxygen functionalization of MXenes. *ACS Nanoscience Au* **2022,** *2* (5), 433-439.
42. Persson, I.; Halim, J.; Hansen, T. W.; Wagner, J. B.; Darakchieva, V.; Palisaitis, J.; Rosen, J.; Persson, P. O., How much oxygen can a MXene surface take before it breaks? *Advanced Functional Materials* **2020,** *30* (47), 1909005.
43. Huang, S.; Mochalin, V. N., Hydrolysis of 2D transition-metal carbides (MXenes) in colloidal solutions. *Inorganic chemistry* **2019,** *58* (3), 1958-1966.
44. Cao, M.; Wang, F.; Wang, L.; Wu, W.; Lv, W.; Zhu, J., Room temperature oxidation of Ti3C2 MXene for supercapacitor electrodes. *Journal of The Electrochemical Society* **2017,** *164* (14), A3933.
45. Cao, F.; Zhang, Y.; Wang, H.; Khan, K.; Tareen, A. K.; Qian, W.; Zhang, H.; Ågren, H., Recent advances in oxidation stable chemistry of 2D MXenes. *Advanced Materials* **2022,** *34* (13), 2107554.
46. Zheng, Z.; Guo, C.; Wang, E.; He, Z.; Liang, T.; Yang, T.; Hou, X., The oxidation and thermal stability of two-dimensional transition metal carbides and/or carbonitrides (MXenes) and the improvement based on their surface state. *Inorganic Chemistry Frontiers* **2021,** *8* (9), 2164-2182.
47. Zhang, C. J.; Pinilla, S.; McEvoy, N.; Cullen, C. P.; Anasori, B.; Long, E.; Park, S.-H.; Seral-Ascaso, A.; Shmeliov, A.; Krishnan, D., Oxidation stability of colloidal two-dimensional titanium carbides (MXenes). *Chemistry of Materials* **2017,** *29* (11), 4848-4856.
48. Liu, N.; Li, Q.; Wan, H.; Chang, L.; Wang, H.; Fang, J.; Ding, T.; Wen, Q.; Zhou, L.; Xiao, X., High-temperature stability in air of Ti3C2T x MXene-based composite with extracted bentonite. *Nature Communications* **2022,** *13* (1), 5551.
49. Shi, H.; Zhang, P.; Liu, Z.; Park, S.; Lohe, M. R.; Wu, Y.; Shaygan Nia, A.; Yang, S.; Feng, X., Ambient-stable two-dimensional titanium carbide (MXene) enabled by iodine etching. *Angewandte Chemie International Edition* **2021,** *60* (16), 8689-8693.
50. Osti, N. C.; Naguib, M.; Ostadhossein, A.; Xie, Y.; Kent, P. R.; Dyatkin, B.; Rother, G.; Heller, W. T.; Van Duin, A. C.; Gogotsi, Y., Effect of metal ion intercalation on the structure of MXene and water dynamics on its internal surfaces. *ACS applied materials & interfaces* **2016,** *8* (14), 8859-8863.
51. Ghidiu, M.; Kota, S.; Drozd, V.; Barsoum, M. W., Pressure-induced shear and interlayer expansion in Ti3C2 MXene in the presence of water. *Science Advances* **2018,** *4* (1), eaao6850.
52. Li, Z.; Wang, L.; Sun, D.; Zhang, Y.; Liu, B.; Hu, Q.; Zhou, A., Synthesis and thermal stability of two-dimensional carbide MXene Ti3C2. *Materials Science and Engineering: B* **2015,** *191*, 33-40.
53. Naguib, M.; Mashtalir, O.; Lukatskaya, M. R.; Dyatkin, B.; Zhang, C.; Presser, V.; Gogotsi, Y.; Barsoum, M. W., One-step synthesis of nanocrystalline transition metal oxides on thin sheets of disordered graphitic carbon by oxidation of MXenes. *Chemical communications* **2014,** *50* (56), 7420-7423.
54. Ghassemi, H.; Harlow, W.; Mashtalir, O.; Beidaghi, M.; Lukatskaya, M.; Gogotsi, Y.; Taheri, M. L., In situ environmental transmission electron microscopy study of oxidation of two-dimensional Ti 3 C 2 and formation of carbon-supported TiO 2. *Journal of Materials Chemistry A* **2014,** *2* (35), 14339-14343.

55. Halim, J.; Persson, I.; Moon, E. J.; Kühne, P.; Darakchieva, V.; Persson, P. O. Å.; Eklund, P.; Rosen, J.; Barsoum, M. W., Electronic and optical characterization of 2D Ti2C and Nb2C (MXene) thin films. *Journal of Physics: Condensed Matter* **2019,** *31* (16), 165301.
56. Yim, C.; O'Brien, M.; McEvoy, N.; Winters, S.; Mirza, I.; Lunney, J. G.; Duesberg, G. S., Investigation of the optical properties of MoS2 thin films using spectroscopic ellipsometry. *Applied Physics Letters* **2014,** *104* (10), 103114.
57. Song, B.; Hou, J.; Wang, H.; Sidhik, S.; Miao, J.; Gu, H.; Zhang, H.; Liu, S.; Fakhraai, Z.; Even, J., Determination of dielectric functions and exciton oscillator strength of two-dimensional hybrid perovskites. *ACS Materials Letters* **2020,** *3* (1), 148-159.
58. Glor, E. C.; Ferrier, R. C.; Li, C.; Composto, R. J.; Fakhraai, Z., Out-of-plane orientation alignment and reorientation dynamics of gold nanorods in polymer nanocomposite films. *Soft Matter* **2017,** *13* (11), 2207-2215.
59. Maguire, S. M.; Bilchak, C. R.; Corsi, J. S.; Welborn, S. S.; Tsaggaris, T.; Ford, J.; Detsi, E.; Fakhraai, Z.; Composto, R. J., Effect of nanoscale confinement on polymer-infiltrated scaffold metal composites. *ACS Applied Materials & Interfaces* **2021,** *13* (37), 44893-44903.
60. Mojtabavi, M.; VahidMohammadi, A.; Ganeshan, K.; Hejazi, D.; Shahbazmohamadi, S.; Kar, S.; Van Duin, A. C.; Wanunu, M., Wafer-scale lateral self-assembly of mosaic Ti3C2T x MXene monolayer films. *ACS nano* **2021,** *15* (1), 625-636.
61. Chaudhuri, K.; Alhabeb, M.; Wang, Z.; Shalaev, V. M.; Gogotsi, Y.; Boltasseva, A., Highly broadband absorber using plasmonic titanium carbide (MXene). *Acs Photonics* **2018,** *5* (3), 1115-1122.
62. Chae, Y.; Kim, S. J.; Cho, S.-Y.; Choi, J.; Maleski, K.; Lee, B.-J.; Jung, H.-T.; Gogotsi, Y.; Lee, Y.; Ahn, C. W., An investigation into the factors governing the oxidation of two-dimensional Ti 3 C 2 MXene. *Nanoscale* **2019,** *11* (17), 8387-8393.
63. Lee, Y.; Kim, S. J.; Kim, Y.-J.; Lim, Y.; Chae, Y.; Lee, B.-J.; Kim, Y.-T.; Han, H.; Gogotsi, Y.; Ahn, C. W., Oxidation-resistant titanium carbide MXene films. *Journal of Materials Chemistry A* **2020,** *8* (2), 573-581.
64. Hosseini Jebeli, S. A.; West, C. A.; Lee, S. A.; Goldwyn, H. J.; Bilchak, C. R.; Fakhraai, Z.; Willets, K. A.; Link, S.; Masiello, D. J., Wavelength-dependent photothermal imaging probes nanoscale temperature differences among subdiffraction coupled plasmonic nanorods. *Nano Letters* **2021,** *21* (12), 5386-5393.
65. Han, M.; Shuck, C. E.; Rakhmanov, R.; Parchment, D.; Anasori, B.; Koo, C. M.; Friedman, G.; Gogotsi, Y., Beyond Ti3C2T x: MXenes for electromagnetic interference shielding. *ACS nano* **2020,** *14* (4), 5008-5016.
66. Li, Q.; Liu, M.; Zhong, B.; Zhang, W.; Jia, Z.; Jia, D., Tetramethylammonium hydroxide modified MXene as a functional nanofiller for electrical and thermal conductive rubber composites. *Composites Communications* **2022,** *34*, 101249.
67. Anupma Thakur, N. C. B. S., Karis Davidson, Annabelle Bedford, Hui Fang, Yooran Im, Vaishnavi Kanduri, Brian C. Wyatt, Srinivasa Kartik Nemani, Zahra Fakhraai, and Babak Anasori, Step-by-step guide for synthesis and delamination of Ti3C2Tx MXene. *Small Methods- Submitted* **2023**.
68. Anasori, B.; Shi, C.; Moon, E. J.; Xie, Y.; Voigt, C. A.; Kent, P. R.; May, S. J.; Billinge, S. J.; Barsoum, M. W.; Gogotsi, Y., Control of electronic properties of 2D carbides (MXenes) by manipulating their transition metal layers. *Nanoscale Horizons* **2016,** *1* (3), 227-234.
69. Walther, M.; Cooke, D.; Sherstan, C.; Hajar, M.; Freeman, M.; Hegmann, F., Terahertz conductivity of thin gold films at the metal-insulator percolation transition. *Physical Review B* **2007,** *76* (12), 125408.
70. Paulite, M.; Fakhraai, Z.; Li, I. T.; Gunari, N.; Tanur, A. E.; Walker, G. C., Imaging secondary structure of individual amyloid fibrils of a β2-microglobulin fragment using near-field infrared spectroscopy. *Journal of the American Chemical Society* **2011,** *133* (19), 7376-7383.

71. Enyashin, A.; Ivanovskii, A., Two-dimensional titanium carbonitrides and their hydroxylated derivatives: Structural, electronic properties and stability of MXenes Ti3C2− xNx (OH) 2 from DFTB calculations. *Journal of Solid State Chemistry* **2013,** *207*, 42-48.
72. Wang, H.-W.; Naguib, M.; Page, K.; Wesolowski, D. J.; Gogotsi, Y., Resolving the structure of Ti3C2T x MXenes through multilevel structural modeling of the atomic pair distribution function. *Chemistry of Materials* **2016,** *28* (1), 349-359.
73. Hope, M. A.; Forse, A. C.; Griffith, K. J.; Lukatskaya, M. R.; Ghidiu, M.; Gogotsi, Y.; Grey, C. P., NMR reveals the surface functionalisation of Ti 3 C 2 MXene. *Physical Chemistry Chemical Physics* **2016,** *18* (7), 5099-5102.
74. Seredych, M.; Shuck, C. E.; Pinto, D.; Alhabeb, M.; Precetti, E.; Deysher, G.; Anasori, B.; Kurra, N.; Gogotsi, Y., High-temperature behavior and surface chemistry of carbide MXenes studied by thermal analysis. *Chemistry of Materials* **2019,** *31* (9), 3324-3332.
75. Magne, D.; Mauchamp, V.; Célérier, S.; Chartier, P.; Cabioc'h, T., Site-projected electronic structure of two-dimensional Ti 3 C 2 MXene: the role of the surface functionalization groups. *Physical Chemistry Chemical Physics* **2016,** *18* (45), 30946-30953.
76. Colin-Ulloa, E.; Fitzgerald, A.; Montazeri, K.; Mann, J.; Natu, V.; Ngo, K.; Uzarski, J.; Barsoum, M. W.; Titova, L. V., Ultrafast Spectroscopy of Plasmons and Free Carriers in 2D MXenes. *Advanced Materials* **2023,** *35* (8), 2208659.
77. Wang, A.; Li, S.; Zhang, X.; Bao, H., Roles of electrons on the thermal transport of 2D metallic MXenes. *Physical Review Materials* **2022,** *6* (1), 014009.
78. Lipatov, A.; Lu, H.; Alhabeb, M.; Anasori, B.; Gruverman, A.; Gogotsi, Y.; Sinitskii, A., Elastic properties of 2D Ti3C2T x MXene monolayers and bilayers. *Science advances* **2018,** *4* (6), eaat0491.
79. Xu, H.; Yin, X.; Li, X.; Li, M.; Zhang, L.; Cheng, L., Thermal stability and dielectric properties of 2D Ti2C MXenes via annealing under a gas mixture of Ar and H2 atmosphere. *Functional Composites and Structures* **2019,** *1* (1), 015002.
80. Kim, H.; Anasori, B.; Gogotsi, Y.; Alshareef, H. N., Thermoelectric properties of two-dimensional molybdenum-based MXenes. *Chemistry of Materials* **2017,** *29* (15), 6472-6479.
81. Anasori, B.; Dahlqvist, M.; Halim, J.; Moon, E. J.; Lu, J.; Hosler, B. C.; Caspi, E. a. N.; May, S. J.; Hultman, L.; Eklund, P., Experimental and theoretical characterization of ordered MAX phases Mo2TiAlC2 and Mo2Ti2AlC3. *Journal of Applied Physics* **2015,** *118* (9), 094304.
82. Anayee, M.; Kurra, N.; Alhabeb, M.; Seredych, M.; Hedhili, M. N.; Emwas, A.-H.; Alshareef, H. N.; Anasori, B.; Gogotsi, Y., Role of acid mixtures etching on the surface chemistry and sodium ion storage in Ti 3 C 2 T x MXene. *Chemical Communications* **2020,** *56* (45), 6090-6093.
83. Yao, L.; Tian, X.; Cui, X.; Zhao, R.; Xiao, X.; Wang, Y., Partially oxidized Ti 3 C 2 T x MXene-sensitive material-based ammonia gas sensor with high-sensing performances for room temperature application. *Journal of Materials Science: Materials in Electronics* **2021,** *32*, 27837-27848.

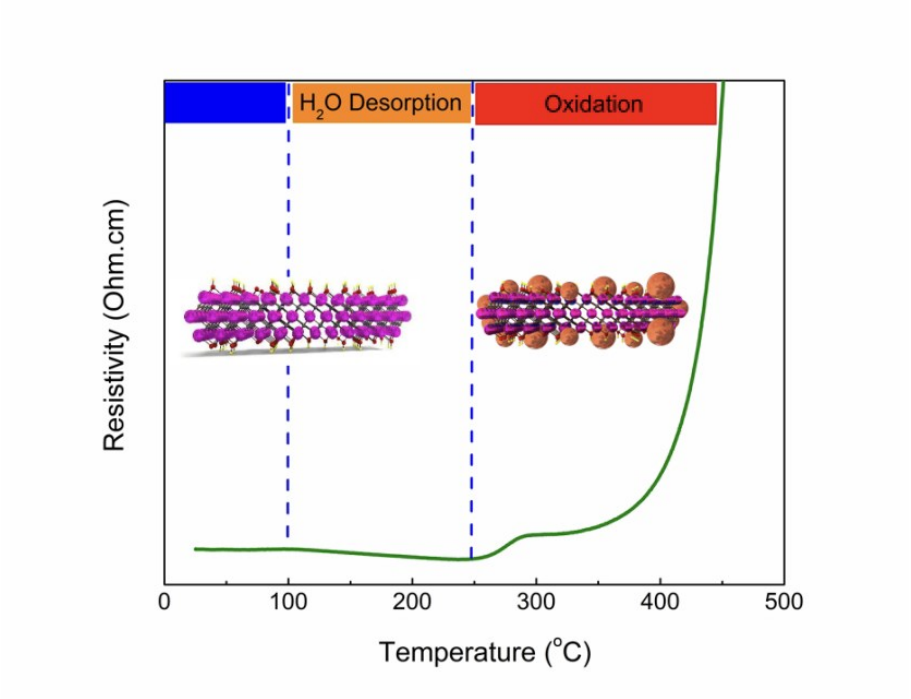
H2O Desorption
Oxidation
Resistivity (Ohm.cm)
0
100
200
300
400
500
Temperature (°C)

TOC